ELSEVIER

Surface and Coatings Technology 113 (1999) 17–24

SURFACE & COATINGS TECHNOLOGY

Gas nitriding of an equiatomic TiNi shape-memory alloy Part I: Nitriding parameters and microstructure characterization

S.K. Wu [a,*], H.C. Lin [b], C.Y. Lee [a]

[a] *Institute of Materials Science and Engineering, National Taiwan University, Taipei, Taiwan, ROC 106*
[b] *Department of Materials Science, Feng Chia University, Taichung, Taiwan, ROC 407*

Received 7 August 1998; accepted 5 November 1998

Abstract

$Ti_{50}Ni_{50}$ shape-memory alloy is gas-nitrided to modify the surface condition. The phases and microstructures of the nitrided surface are studied by using X-ray diffraction, electron probe microanalysis and scanning electron microscopy. Experimental results indicate that the specimen nitrided at 900 °C exhibits a smooth surface morphology, but for the specimen nitrided at 600 °C, a large number of surface cracks exist. The weight gains of specimens nitrided at temperatures below 650 °C are much higher than those of specimens nitrided at temperatures above 700 °C. These weight gains are found to increase gradually with an increase in nitriding time, and then approach saturated values at 24 h. The 900 °C nitrided specimen consists of TiN and $Ti_2NiH_{0.5}$, two distinct layers. The surface layer of the 600 °C nitrided specimen has two regions: one is a random mixture of TiN, $Ti_2NiH_{0.5}$ and a nickel-rich phase, the other is a columnar-like structure of mixed TiN and nickel-rich phase. Reaction mechanisms to explain the formation of gas-nitrided layers at 600 °C and 900 °C are also examined in this study.

Keywords: Gas nitriding; TiNi shape-memory alloy; Microstructure characterization

1. Introduction

TiNi alloys are known as the most important shape-memory alloys (SMAs) and have many applications that are based on their shape-memory effect (SME) [1] and pseudoelasticity (PE) [2,3]. This stems from the fact that TiNi alloys have superior properties in ductility, biocompatibility and recoverable strain. Recently, TiNi alloys were observed to exhibit good wear resistance [4–6], which is an important property in some biomedical applications such as medical guide-wires, artificial bone joints, etc. In fact, the B2 phase (austenite parent phase) of TiNi alloys exhibits excellent wear resistance due to its rapid work hardening and pseudoelastic properties [7]. However, the wear resistance of the B19′ phase (martensite phase) is still too low and needs to be improved for some applications.

It is well known that nitriding techniques are commonly used to improve the fatigue and wear resistance of metals and alloys [8]. Moine et al. [9] have also tried to increase the wear resistance of TiNi alloys by N^+-ion implantation. In previous work [10,11] we investigated the ion nitriding of TiNi alloys, including the nitriding parameters, microstructure characterization, corrosion and wear properties. In the present study, the gas-nitriding technique has been successfully used to form a nitrided layer on the equiatomic TiNi alloy. The gas-nitriding parameters and the characteristics of the nitrided layers are discussed in the first paper in this series. The surface hardness, wear characteristics, transformation temperature and shape-memory ability of nitrided layers are discussed in the second paper.

2. Experimental procedures

The conventional tungsten arc-melting technique was employed to prepare the equiatomic TiNi alloy. Titanium (purity, 99.7%) and nickel (purity 99.98%), weighing approximately 100 g in total, were melted and remelted at least six times in an argon atmosphere. Pure titanium buttons were also melted and used as getters. The mass loss during melting was negligibly small. The

* Corresponding author. Tel: +886 2 2363 7846; Fax: +886 2 2363 4562; e-mail: skw@ccms.ntu.edu.tw

0257-8972/99/$ – see front matter
PII S0257-8972(98)00811-1

as-melted buttons were homogenized at 1000 °C in a vacuum furnace at 7×10^{-6} Torr for 72 h, and then hot-rolled into plates of 1.5 mm thickness. Specimens with dimensions 30 mm × 10 mm × 1.5 mm were then cut from these plates with a low-speed diamond saw, and then annealed at 800 °C in a vacuum furnace for 2 h. Before gas nitriding, the specimen surfaces were polished with 2000 grit emery paper and cleaned ultrasonically in acetone to remove surface grease. Gas nitriding was carried out in a self-assembled furnace as illustrated in Fig. 1. The nitriding parameters employed in this study are presented in Table 1.

The microstructure of the nitrided layers was studied by X-ray diffraction (XRD) and scanning electron microscopy (SEM). XRD tests were carried out on a Philips PW 1710 XRD instrument using Cu Kα radiation. The power was 40 kV × 30 mA and the 2θ scanning rate was 3° min^{-1}. The surface morphologies and cross-sections of nitrided samples were observed in a Philips 515 SEM with an energy-dispersive spectroscopy (EDX) facility. The chemical compositions of surface layers were then analyzed with a JEOL JXA-8600SX electron probe microanalyzer (EPMA) having a probe size of 1 μm. The nitrogen and hydrogen concentrations of the nitrided surface layers were measured with Leco TC-136 type and Leco RH-404 type analyzers, respectively.

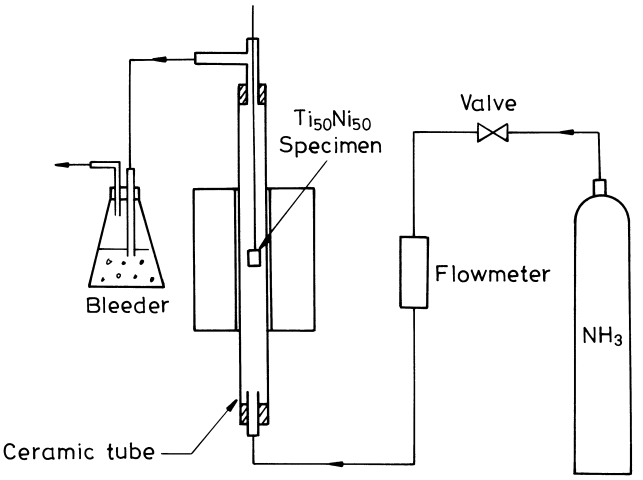

Fig. 1. Schematic illustration of the gas-nitriding equipment using in the present study.

Table 1
Nitriding parameters employed in the present study

Specimen no.	Nitriding emperature (°C)	Nitriding time (h)	NH_3 flow rate (cm^3 min^{-1})
1	600	1	50
2	600	2	50
3	600	4	50
4	600	8	50
5	600	16	50
6	600	24	50
7	650	24	50
8	700	24	50
9	750	24	50
10	800	24	50
11	850	24	50
12	900	4	50
13	900	8	50
14	900	16	50
15	900	24	50
16	950	24	50
17	1000	24	50

3. Results and discussion

3.1. Microstructures and composition analysis of gas-nitrided $Ti_{50}Ni_{50}$ alloy

3.1.1. Surface morphologies and weight gains

After gas nitriding, $Ti_{50}Ni_{50}$ specimens show homogeneous surface morphologies, with colors ranging from purple to golden yellow, with an increase in the nitriding temperature. The homogeniety and surface roughness are dependent on the nitriding parameters, as shown in Fig. 2(a) and (b) for $Ti_{50}Ni_{50}$ specimens nitrided at 600 °C and 900 °C, respectively. A smooth surface morphology can be seen in Fig. 2(b), but many surface cracks are observed in Fig. 2(a). The longer the nitriding time at 600 °C, the more surface cracks appear. These surface cracks are attributed to the large difference between the thermal expansion coefficients of the nitrided layer and the $Ti_{50}Ni_{50}$ matrix, and to the effect of hydrogen embrittlement resulting from the existence of numerous hydrogen atoms on the nitrided layer.

Fig. 3 shows the weight gain per unit area versus nitriding temperature for $Ti_{50}Ni_{50}$ specimens subjected to 24 h of gas nitriding. This weight gain originates from the formation of a nitrided layer on the specimen surface and is proportional to the thickness of the nitrided layer. From Fig. 3, one can find that the weight gains of $Ti_{50}Ni_{50}$ specimens nitrided at temperatures below 650 °C are much higher than those of specimens nitrided at temperatures above 700 °C. The specimen nitrided at 800 °C has the smallest weight gain. Fig. 4 shows the weight gain per unit area versus nitriding time for $Ti_{50}Ni_{50}$ specimens subjected to gas nitriding at 600 °C and 900 °C. In Fig. 4, the weight gains per unit area increase gradually with increasing nitriding time, and then approach saturated values for both 600 °C and 900 °C nitrided specimens. However, a more rapid weight gain is exhibited for specimens gas-nitrided at 600 °C than for those at 900 °C. These features, shown in Figs. 3 and 4, indicate that the gas nitriding of $Ti_{50}Ni_{50}$ specimens may exhibit a different reaction mechanism at low and high nitriding temperatures, as discussed in Section 3.2.

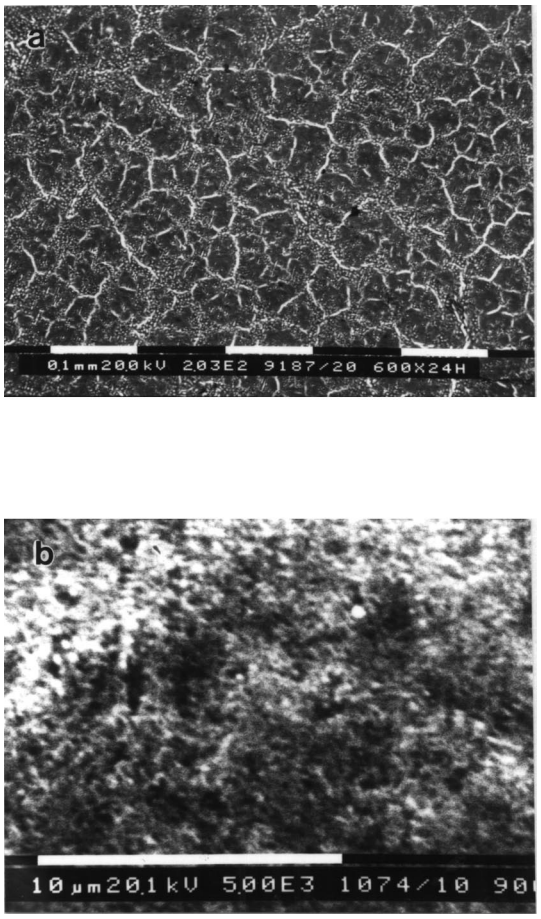

Fig. 2. Scanning electron micrographs of the surface morphology of $Ti_{50}Ni_{50}$ specimens after gas nitriding at (a) 600 °C and (b) 900 °C for 24 h.

3.1.2. XRD analysis

In order to better understand the gas nitriding of $Ti_{50}Ni_{50}$ specimens, XRD measurements were used to investigate the nitrided layers. Figs. 5 and 6 show the XRD patterns of the surfaces of $Ti_{50}Ni_{50}$ specimens subjected to gas nitriding at 600 °C and 900 °C, respectively, from 1 to 24 h. The XRD peaks of TiN and $Ti_2NiH_{0.5}$ compounds are clearly observed in Figs. 5 and 6. It is reported [10] that not only TiN, but also

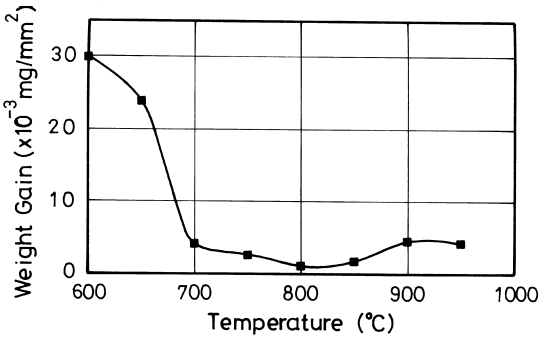

Fig. 3. Weight gain versus nitriding temperature for $Ti_{50}Ni_{50}$ specimens subjected to gas nitriding for 24 h.

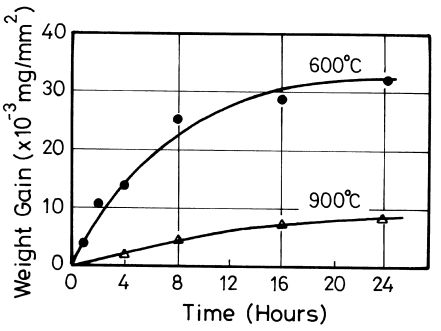

Fig. 4. Weight gain versus nitriding time for $Ti_{50}Ni_{50}$specimens subjected to gas nitriding at 600 °C and 900 °C.

the compound Ti_2Ni will appear after ion nitriding of $Ti_{50}Ni_{50}$ specimens. In the present study, we believe that Ti_2Ni will also form simultaneously with TiN during the gas nitriding of $Ti_{50}Ni_{50}$ specimens. In the meantime, the NH_3 gas is decomposed into hydrogen and nitrogen atoms during gas nitriding. The Ti_2Ni easily adsorbs hydrogen atoms to form Ti_2Ni–H [12]. Hence, the TiN and $Ti_2NiH_{0.5}$ compounds will form concurrently in the gas-nitrided layers of $Ti_{50}Ni_{50}$ specimens. Because the nitrided layers are quite thin for the 900 °C nitrided specimens, the $Ti_{50}Ni_{50}$ matrix can also be diffracted, and B19′ martensite appears as evidenced by its XRD peaks in Fig. 6. However, the nitrided layers

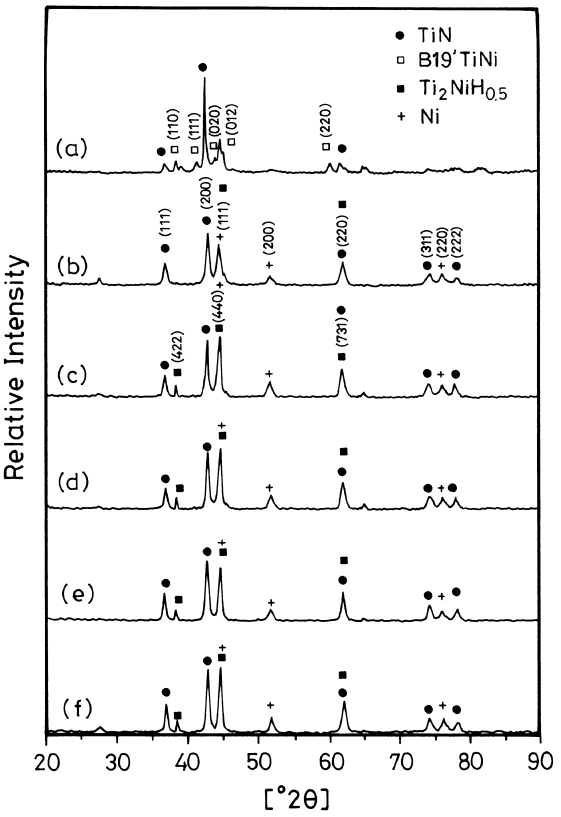

Fig. 5. XRD patterns of $Ti_{50}Ni_{50}$ specimens after nitriding at 600 °C for (a) 1 h, (b) 2 h, (c) 4 h, (d) 8 h, (e) 16 h and (f) 24 h.

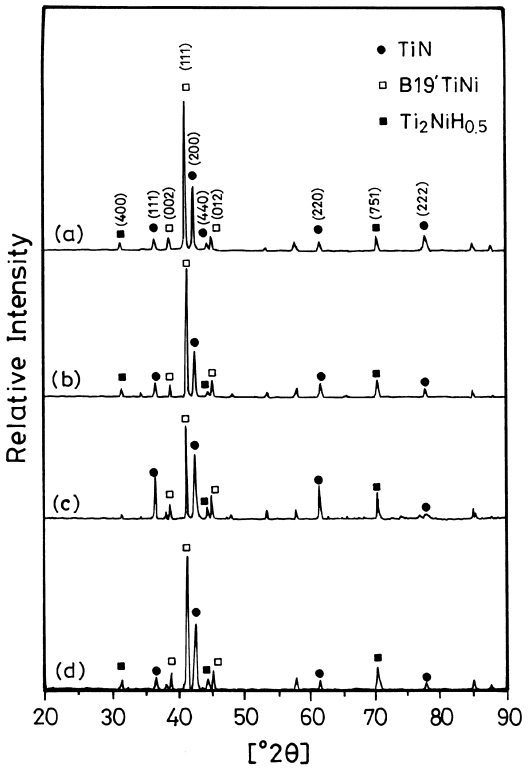

Fig. 6. XRD patterns of $Ti_{50}Ni_{50}$ specimens after nitriding at 900 °C for (a) 4 h, (b) 8 h, (c) 16 h and (d) 24 h.

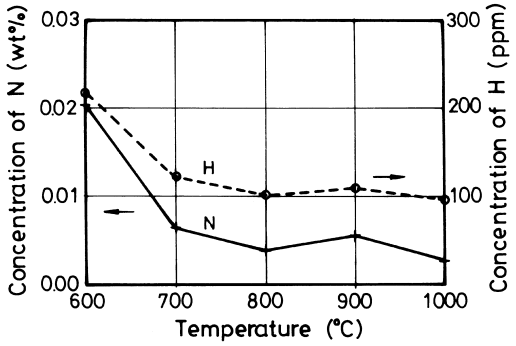

Fig. 7. Concentrations of nitrogen and hydrogen versus nitriding temperature for $Ti_{50}Ni_{50}$ specimens subjected to gas nitriding for 24 h.

are so thick for the 600 °C nitrided specimens (except for the 600 °C × 1 h nitrided specimen), as revealed from the large weight gain in Fig. 4, that the $Ti_{50}Ni_{50}$ matrix cannot be diffracted, and hence no XRD peaks attributable to B19′ martensite appear in Fig. 5. As seen in Fig. 5(a), only a thin TiN compound layer forms on the nitrided surface. In addition to the appearance of TiN and $Ti_2NiH_{0.5}$ compounds, the XRD peaks of a nickel-rich phase are also observed in Fig. 5, but not in Fig. 6. Due to the formation of TiN and $Ti_2NiH_{0.5}$ in the nitrided layer, many titanium atoms of the $Ti_{50}Ni_{50}$ matrix have been exhausted and the retained nickel atoms will be clustered. At 600 °C, these nickel clusters will dissolve into a few atoms of titanium, nitrogen and hydrogen to form a nickel-rich solid solution. For the 900 °C nitrided specimens, the retained nickel atoms will diffuse into the $Ti_{50}Ni_{50}$ matrix because both the diffusion rate and the saturated quantity of dissolved nickel atoms in the $Ti_{50}Ni_{50}$ matrix are much higher at 900 °C, and hence the nickel-rich phase does not appear in Fig. 6.

3.1.3. Nitrogen and hydrogen concentrations in nitrided layers

Fig. 7 shows the concentrations of nitrogen and hydrogen in nitrided layers for the $Ti_{50}Ni_{50}$ specimens subjected to 24 h of gas nitriding at various temperatures. The concentrations of nitrogen and hydrogen were examined by using 5 mm × 5 mm × 1 mm specimens cut from the gas-nitrided specimens. In Fig. 7, the highest concentrations of nitrogen and hydrogen appear for specimens nitrided at 600 °C, lower concentrations being observed for specimens nitrided at 700–1000 °C. These characteristics shown in Fig. 7 can be explained as follows. As mentioned above, thicker nitrided layers are formed by gas nitriding at temperatures below 650 °C. These nitrided layers are mainly TiN and $Ti_2NiH_{0.5}$ compounds, as indicated in Fig. 5. Hence, higher concentrations of nitrogen and hydrogen for 600 °C nitrided specimens exist due to their thicker nitrided layer. In the same way, the lower concentration of nitrogen and hydrogen for 700–1000 °C nitrided specimens is due to their thinner nitrided layer.

3.1.4. Cross-sectional SEM micrographs and EPMA analysis

Cross-sectional SEM micrographs of $Ti_{50}Ni_{50}$ specimens nitrided at 900 °C for 12 and 24 h are shown in Fig. 8(a) and (b), respectively. On carefully examining Fig. 8, two different layers — an outer layer labeled A and an inner layer labeled B — are formed on the nitrided specimens. These nitrided layers are the compound layers often seen in nitrided pure titanium and titanium alloys [10,11,13–25]. As observed from the XRD patterns in Fig. 6, these nitrided layers should be related to the TiN and $Ti_2NiH_{0.5}$ compounds. The concentration profiles of titanium, nickel and nitrogen in these nitrided layers of $Ti_{50}Ni_{50}$ specimens were examined by EPMA. Fig. 9 shows the EPMA line scan of a $Ti_{50}Ni_{50}$ specimen nitrided at 900 °C for 24 h. The intensity of the N Kα line increases from the surface to a maximum at the position of the outer compound layer (layer A) and then levels off at the interface of layers A and B. The intensity of the Ti Kα line also increases from the surface to a maximum at layer A, decreases to an intermediate intensity through layer B and then levels off at the interface between layer B and the $Ti_{50}Ni_{50}$ matrix. The intensity of the Ni Kα line in layer A is rather weak. It increases to an intermediate intensity

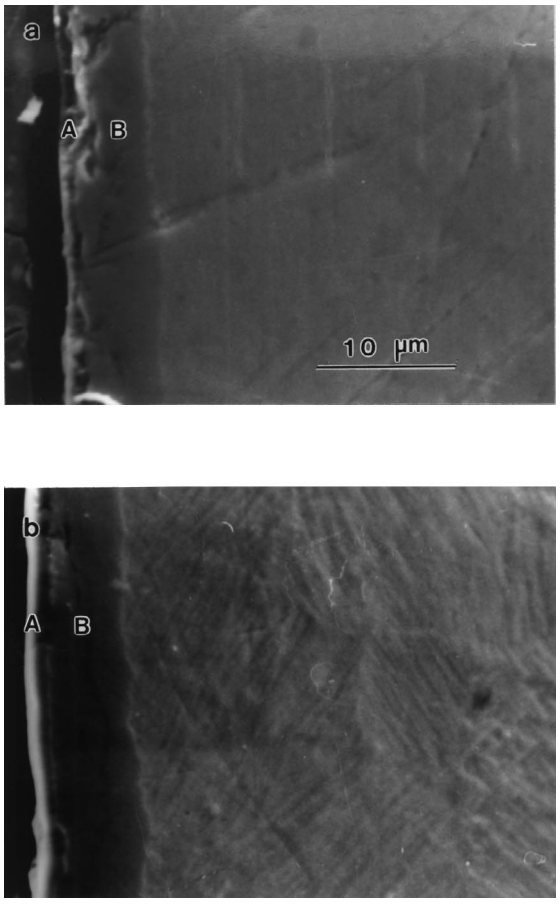

Fig. 8. Scanning electron micrographs of cross-sections of $Ti_{50}Ni_{50}$specimens after gas nitriding at 900 °C for (a) 12 h and (b) 24 h.

through layer B and then increases to a higher intensity at the interface between layer B and the $Ti_{50}Ni_{50}$ matrix. From the results of Figs. 6 and 9, we propose that layer A is a TiN compound and layer B is a $Ti_2NiH_{0.5}$ compound for 900 °C nitrided $Ti_{50}Ni_{50}$ specimens, although hydrogen atoms cannot be detected by using the EPMA. It is difficult to confirm the existence of nitrogen in the $Ti_2NiH_{0.5}$ compound layer because of the very low nitrogen concentration in this layer.

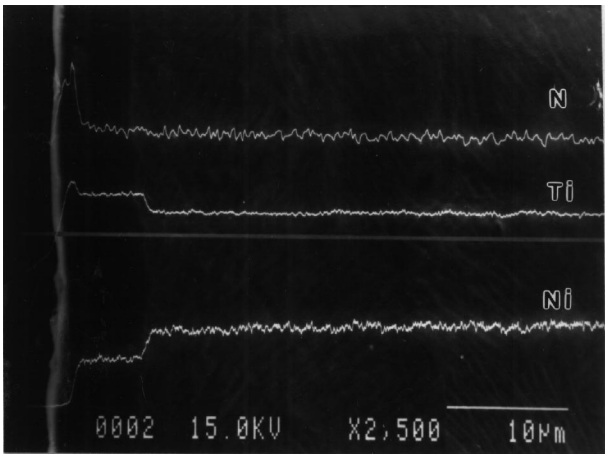

Fig. 9. EPMA line-scan profiles of a $Ti_{50}Ni_{50}$ specimen after gas nitriding at 900 °C for 24 h.

We are also interested in the kinds of nitrided layers that appear in the $Ti_{50}Ni_{50}$ specimens nitrided at 600 °C. The cross-sectional SEM micrographs of $Ti_{50}Ni_{50}$ specimens nitrided at 600 °C are shown in Fig. 10(a)–(e). From Fig. 10(a) and (b), one can find that the reaction interface between the nitrided layer and the $Ti_{50}Ni_{50}$ matrix is flat in the first 2 h of nitriding. However, there is a wavy reaction interface between the nitrided layer and $Ti_{50}Ni_{50}$ matrix after 4 h of nitriding, as shown in Fig. 10(c)–(e). As indicated by the arrows in Fig. 10(c), some black points appear, which are identified by EDX to be a compound comprised of titanium and nitrogen atoms. As the nitriding time increases, these black points increase continuously, advance into the $Ti_{50}Ni_{50}$ matrix and then form black and white columnar-like morphologies, as shown in Fig. 10(d) and (e).

Fig. 11(a) and (b) show the EPMA image and line scan of the $Ti_{50}Ni_{50}$ specimen nitrided at 600 °C for 24 h. In Fig. 11(a), two distinct regions appear (I and II) in the nitrided layers. The thicknesses of regions I and II are approximately 30 μm and 40 μm, respectively. In region I, the intensities of Ti and Ni Kα lines vary greatly, although the N Kα line maintains a somewhat higher intensity than that observed in the $Ti_{50}Ni_{50}$ matrix, as shown in Fig. 11(b). This indicates that the composition is not homogeneous in this region. Compared with the XRD results shown in Fig. 5, region I should be composed of a mixture of TiN, $Ti_2NiH_{0.5}$ and a nickel-rich phase. In region II, black and white columnar-like images can be seen. In the white region, the intensities of the Ti and N Kα lines are quite small, and the intensity of the Ni Kα line is higher than that of the $Ti_{50}Ni_{50}$ matrix. However, in the black region, the intensity of the Ni Kα line has obviously decreased, and the intensities of the Ti and N Kα lines are higher than those of the $Ti_{50}Ni_{50}$ matrix. Based on these EPMA analyses and the XRD results of Fig. 5, the black region in region II is believed to be a TiN compound and the white region, a nickel-rich phase. These features will be discussed more in the next section.

3.2. Gas-nitriding mechanism in equiatomic TiNi shape-memory alloy

3.2.1. Gas nitriding at 900 °C

To explain the reaction of $Ti_{50}Ni_{50}$ alloy gas-nitrided at 900 °C, we propose a three-step mechanism as shown schematically in Fig. 12. During gas nitriding, the NH_3 gas decomposes into nitrogen and hydrogen atoms [Fig. 12(a)]. Because the chemical affinity of titanium and nitrogen is much stronger than that of nickel and nitrogen [26], the reaction of nitrogen and titanium atoms occurs more easily than that of nitrogen and

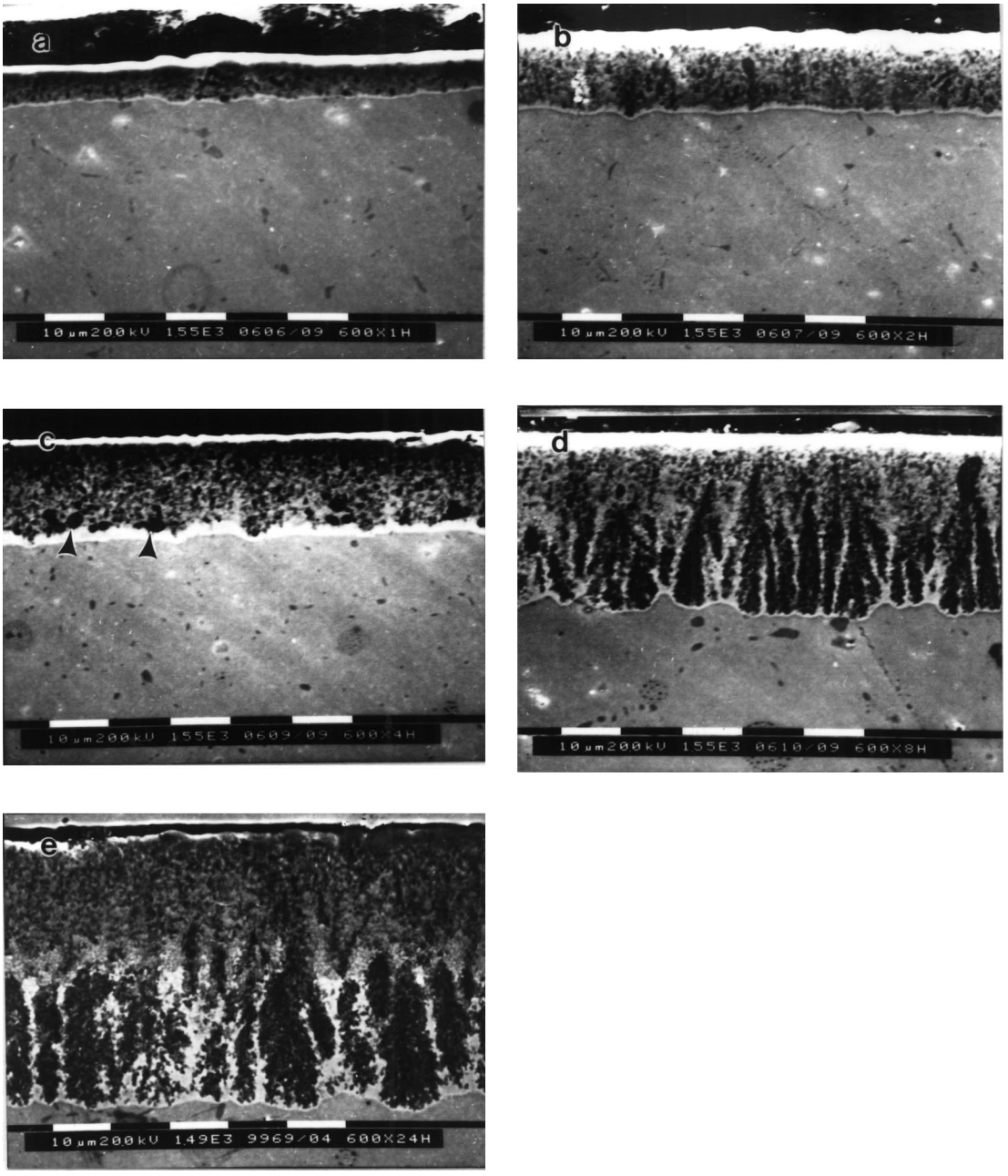

Fig. 10. Scanning electron micrographs of cross-sections of $Ti_{50}Ni_{50}$specimens after gas nitriding at 600 °C for (a) 1 h, (b) 2 h, (c) 4 h, (d) 8 h and (e) 24 h.

nickel atoms. This means that the layer formed on the specimen surface is composed of a greater amount of TiN than Ni*x*N, as shown in layer A of Fig. 12(b). We believe that the Ni*x*N phase is not found in the XRD results of Fig. 6 because the amount of Ni*x*N is too small to be detected. As the process continues, the nitrogen and hydrogen atoms in layer A diffuse inwards. The titanium atoms can react more easily with nitrogen; thus an outward driving force of titanium atoms, together with the inward movement of nitrogen atoms, forms TiN and thickens layer A. Meanwhile, the outward-moving titanium atoms will react with TiNi to form the compound Ti_2Ni. This Ti_2Ni will easily adsorb the inward-moving hydrogen atoms to form the $Ti_2NiH_{0.5}$ layer [layer B of Fig. 12(c)]. When the TiN in layer A reaches a certain thickness, it may become a barrier [27,28] and subsequently reduce the diffusion of nitrogen atoms into the $Ti_2NiH_{0.5}$ layer. This feature also reflects the undetectable nitrogen concentration at the inner part of layer B and in the $Ti_{50}Ni_{50}$ matrix.

3.2.2. Gas nitriding at 600 °C

We also wish to propose a reaction mechanism of a 600 °C gas-nitrided $Ti_{50}Ni_{50}$ specimen. As illustrated in

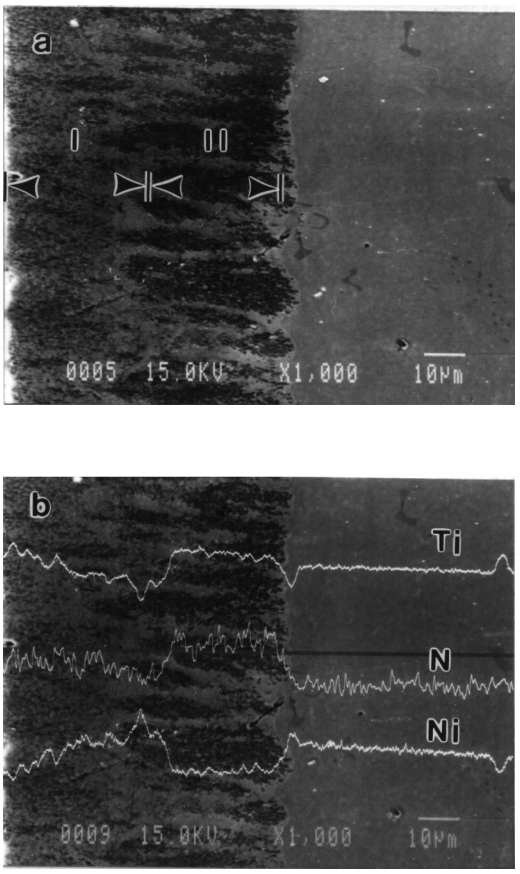

Fig. 11. (a) Scanning electron micrograph of the cross-section and (b) EPMA line-scan profiles of a $Ti_{50}Ni_{50}$ specimen after gas nitriding at 600 °C for 24 h.

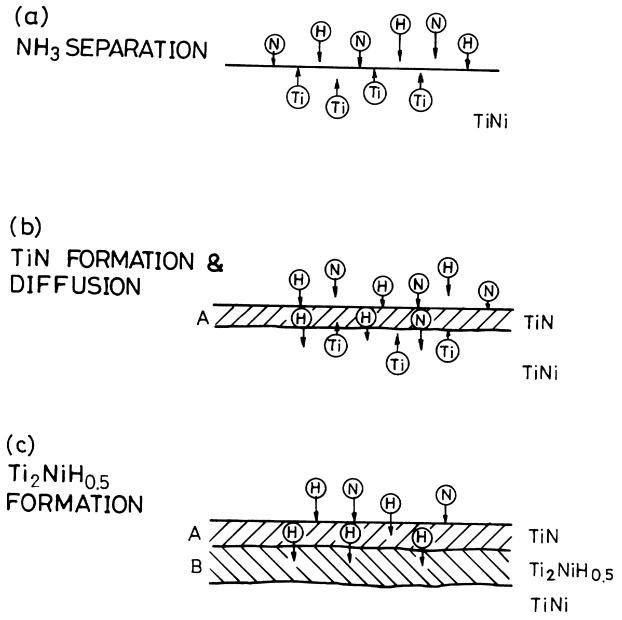

Fig. 12. Schematic diagram of the reaction mechanism of a $Ti_{50}Ni_{50}$ specimen nitrided at 900 °C.

Fig. 13(a), TiN and $Ti_2NiH_{0.5}$ compounds are randomly mixed in the outer surface region and the nickel-rich phase precipitates in the inner region near the $Ti_{50}Ni_{50}$ matrix. Compared with the 900 °C nitrided $Ti_{50}Ni_{50}$ specimen, the 600 °C nitrided specimen does not exhibit distinguishable TiN and $Ti_2NiH_{0.5}$ compound layers. This feature can be explained as follows. During gas nitriding, the TiN compound exhibits much higher nucleation and growth rates than the $Ti_2NiH_{0.5}$ compound at 900 °C; however, TiN and $Ti_2NiH_{0.5}$ compounds are expected to have similar nucleation and growth rates at 600 °C. Hence, TiN and $Ti_2NiH_{0.5}$ compounds appear simultaneously during nitriding at 600 °C. In the meantime, the formation of TiN will increase the quantity of nickel clusters around the TiN and enhance the formation of the nickel-rich phase. Hence, the 600 °C nitrided layer is a random mixture of TiN, $Ti_2NiH_{0.5}$ and nickel-rich phase. This randomly mixed layer increases its thickness with increasing nitriding time, as shown in Fig. 13(b). When the mixed layer reaches a critical thickness, the TiN compound and nickel-rich phase gradually grow inwards into the $Ti_{50}Ni_{50}$ matrix. In this way, the titanium atoms are attracted outwards by the nitrogen atoms, continuously forming the TiN compound. Meanwhile, the nickel atoms left behind in the $Ti_{50}Ni_{50}$ matrix continuously form the nickel-rich phase. Hence, based on this reaction mechanism, the 600 °C nitrided layer consists of two distinct regions: one is a random mixture of TiN,

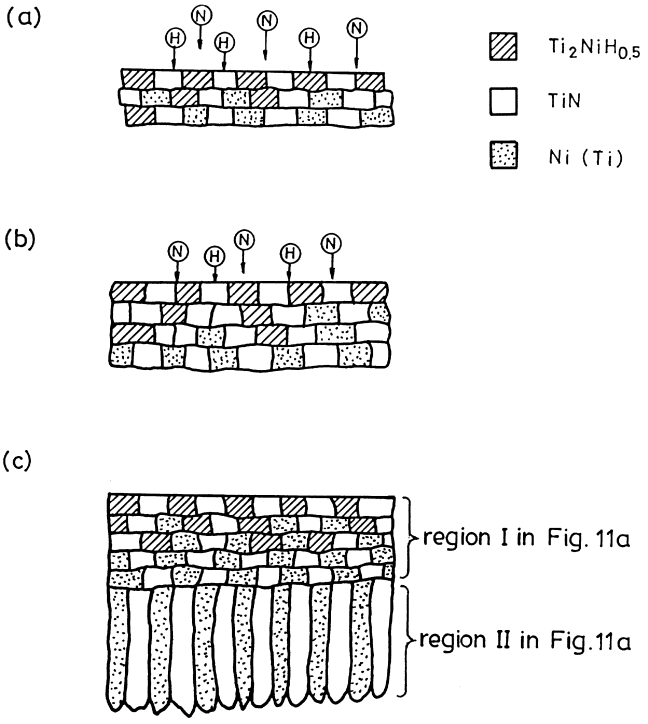

Fig. 13. Schematic diagram of the reaction mechanism of a $Ti_{50}Ni_{50}$ specimen nitrided at 600 °C.

$Ti_2NiH_{0.5}$ and nickel-rich phase [region I in Fig. 11(a)] and the other is composed of columnar-like structures of mixed TiN and nickel-rich phase [region II in Fig. 11(a)], as illustrated in Fig. 13(c). These features are consistent with the results of SEM observation and EPMA analyses in Figs. 10 and 11.

4. Conclusions

The gas nitriding of the $Ti_{50}Ni_{50}$ shape-memory alloy has been investigated by means of weight gain measurements, XRD, SEM and EPMA analyses. The important results can be summarized as follows.

(1) The gas-nitrided $Ti_{50}Ni_{50}$ specimens show homogeneous surface morphologies, with colors ranging from purple to golden yellow, with an increase in the nitriding temperature. A smooth surface morphology appears in the 900 °C nitrided specimens. However, many surface cracks are observed in the 600 °C nitrided specimens.

(2) The weight gains of $Ti_{50}Ni_{50}$ specimens nitrided at temperatures below 650 °C are much higher than those of specimens nitrided at temperatures above 700 °C. Additionally, these weight gains, which are found to increase gradually with an increase in nitriding time, approach saturated values at 24 h.

(3) The 900 °C gas-nitrided $Ti_{50}Ni_{50}$ specimen consists of two distinguishable nitrided layers of TiN and $Ti_2NiH_{0.5}$ compounds. However, the 600 °C gas-nitrided $Ti_{50}Ni_{50}$ specimen consists of two distinct nitrided regions: one is a random mixture of TiN, $Ti_2NiH_{0.5}$ and a nickel-rich phase; the other consists of columnar-like structures of mixed TiN and nickel-rich phase.

(4) The gas-nitriding mechanism of the $Ti_{50}Ni_{50}$ specimen nitrided at 900 °C is suggested to include several simultaneous steps: the decomposition of NH_3 gas to form nitrogen and hydrogen atoms, the formation of TiN compound on the nitrided surface, the diffusion of nitrogen and hydrogen atoms into the matrix, the reaction of titanium and TiNi to form Ti_2Ni, and the reaction of hydrogen and Ti_2Ni to form the $Ti_2NiH_{0.5}$ compound.

(5) For the specimen nitrided at 600 °C, the gas-nitriding mechanism is more complicated. In addition to the TiN and $Ti_2NiH_{0.5}$ compounds, the nickel-rich phase occurs simultaneously to form a random mixture of TiN, $Ti_2NiH_{0.5}$ and a nickel-rich phase in the outer nitrided region. In the inner nitrided region, the enhanced formation of TiN and nickel-rich phase will result in a columnar-like structure of mixed TiN and nickel-rich phase.

Acknowledgement

The authors are pleased to acknowledge the financial support of this research by the National Science Council (NSC), Republic of China, under Grant NSC 84-2216-E-002-027.

References

[1] S. Miyazaki, K. Otsuka, Y. Suzuki, Scripta Metall. 15 (1981) 287–292.
[2] S. Miyazaki, Y. Ohmi, K. Otsuka, Y. Suzuki, J. Phys. 43 (C4) (1982) 255–260. Proc. ICOMAT-82
[3] S. Miyazaki, T. Imai, Y. Igo, K. Otsuka, Metall. Trans. A 17A (1986) 115–120.
[4] J.L. Jin, H.L. Wang, Acta Metall. Sinica 24 (1988) A66–69.
[5] D.Y. Li, Scripta Metall. 34 (1996) 195–200.
[6] P. Clayton, Wear 162–164 (1993) 202–210.
[7] H.C. Lin, H.M. Liao, J.L. He, K.C. Chen, K.M. Lin, Metall. Mater. Trans. A 28A (1997) 1871–1877.
[8] ASM Handbook, 9th ed., vol. 4, American Society for Metals, Metals Park, OH, 1991, p. 387.
[9] P. Moine, O. Popoola, J.P. Villain, Scripta Metall. 20 (1986) 305–310.
[10] S.K. Wu, C.L. Chu, H.C. Lin, Surf. Coatings Technol. 92 (1997) 197–205.
[11] S.K. Wu, C.L. Chu, H.C. Lin, Surf. Coatings Technol. 92 (1997) 206–211.
[12] JCPDS file: 27-346, copyright 1987–1994, JCPDS - ICDD, Newtown Square, PA 19073, USA.
[13] L.H. Chang, L.K. Lee, H.C. Peng, C.Y. Wang, Acta Metall. Sinica 20 (1984) A221–228. in Chinese
[14] A. Raveh, P.L. Hansen, R. Avni, A. Grill, Surf. Coatings Technol. 38 (1989) 339–351.
[15] E. Metin, O.T. Inal, Metall. Trans. A 20 (1989) 1819–1823.
[16] E. Metin, O.T. Inal, Mater. Sci. Eng. A 145 (1991) 65–77.
[17] E. Metin, Scripta Metall. 26 (1992) 1193–1197.
[18] H.J. Brading, P.H. Morton, T. Ell, L.G. Earwaker, Surf. Eng. 8 (1992) 206–212.
[19] A. Ravech, R. Avni, A. Grill, Thin Solid Films 186 (1990) 241–256.
[20] F.M. Kustas, M.S. Misra, R. Wei, P.J. Wilbur, J.A. Knapp, Surf. Coatings Technol. 51 (1992) 100–105.
[21] P. Scradi, B. Tesi, T. Bacci, C. Gianoglio, Surf. Coatings Technol. 41 (1990) 83–91.
[22] K.T. Rie, T. Lampe, Mater. Sci. Eng. 69 (1985) 473–481.
[23] E. Rolinski, Mater. Sci. Eng. 100 (1988) 193–199.
[24] R. Avni, T. Spalvins, Mater. Sci. Eng. 95 (1987) 237–246.
[25] C.L. Chu, S.K. Wu, Surf. Coatings Technol. 78 (1996) 211–226.
[26] C.E. Wicks, F.E. Block, Thermodynamic Properties of 65 Elements — Their Oxides, Halides, Carbides and Nitrides, US Government Printing Office, Washington, DC, 1963, pp. 13–124.
[27] M. Wittmer, Appl. Phys. Lett. 36 (6) (1980) 456–458.
[28] M. Wittmer, Appl. Phys. Lett. 37 (6) (1980) 540–542.